Available online at www.sciencedirect.com

ScienceDirect

journal homepage: www.elsevier.com/locate/ijrefrig

An experimental investigation on the entire pool boiling curve of R14 under 0.1 MPa pressure☆

Ch. Zhao [a,b], M.Q. Gong [a,*], L. Ding [a,b], X. Zou [a], G.F. Chen [a], J.F. Wu [a]

[a] Key Laboratory of Cryogenics, Technical Institute of Physics and Chemistry, Chinese Academy of Sciences, Haidian District, Beijing 100190, China

[b] University of Chinese Academy of Sciences, Beijing 100049, China

ARTICLE INFO

Article history:
Received 30 October 2013
Received in revised form
19 December 2013
Accepted 24 December 2013
Available online 8 January 2014

Keywords:
Entire pool boiling curve
CHF
Pool boiling
R14

ABSTRACT

In this work, the entire pool boiling curve of tetrafluoromethane (R14) under 0.1 MPa was experimentally acquired on a horizontal copper surface, and the nucleate boiling, critical heat flux (CHF) point, transition boiling, Leidenfrost point (the minimum film boiling point) and film boiling were observed. In the nucleate boiling regime, boiling heat transfer data and bubble images depicting the boiling behavior at different heat fluxes were obtained from the measurements. The measured heat flux at the CHF point is 220.39 kW m^{-2}, and the corresponding surface superheat temperature is 16.1 K. The measured CHF data were also compared to several existing correlations, including the Bailey and Lienhard & Dhir correlations, both of which show good agreement. We also measured the boiling heat transfer data in the transition and film boiling regimes. The measured heat flux and surface superheat temperature of the Leidenfrost point were 126.83 kW m^{-2} and 87.1 K, respectively.

Une étude expérimentale sur la courbe entière d'ébullition libre du R14 sous une pression de 0,1 MPa

Mots clés : Courbe entière d'ébullition libre ; Flux thermique critique ; Ebullition en écoulement ; R14

1. Introduction

Boiling heat transfer is an important process in refrigeration and other industrial applications because of its remarkable effectiveness in carrying heat from a heater to a liquid. Experimental research conducted on pool boiling curves is crucial to further understand the boiling mechanism. An entire pool boiling curve is of great interest for both academic investigation and industrial applications. However, entire pool boiling curves are not often found in open published literature, especially for substances with low boiling temperatures.

☆ The original paper was presented at the 5th International Conference on Cryogenics and Refrigeration (ICCR2013), April 6–9, Hangzhou, China.

* *Corresponding author*. Tel./fax: +86 10 82543728.
E-mail address: gongmq@mail.ipc.ac.cn (M.Q. Gong).

0140-7007/$ – see front matter © 2014 Elsevier Ltd and IIR. All rights reserved.
http://dx.doi.org/10.1016/j.ijrefrig.2013.12.014

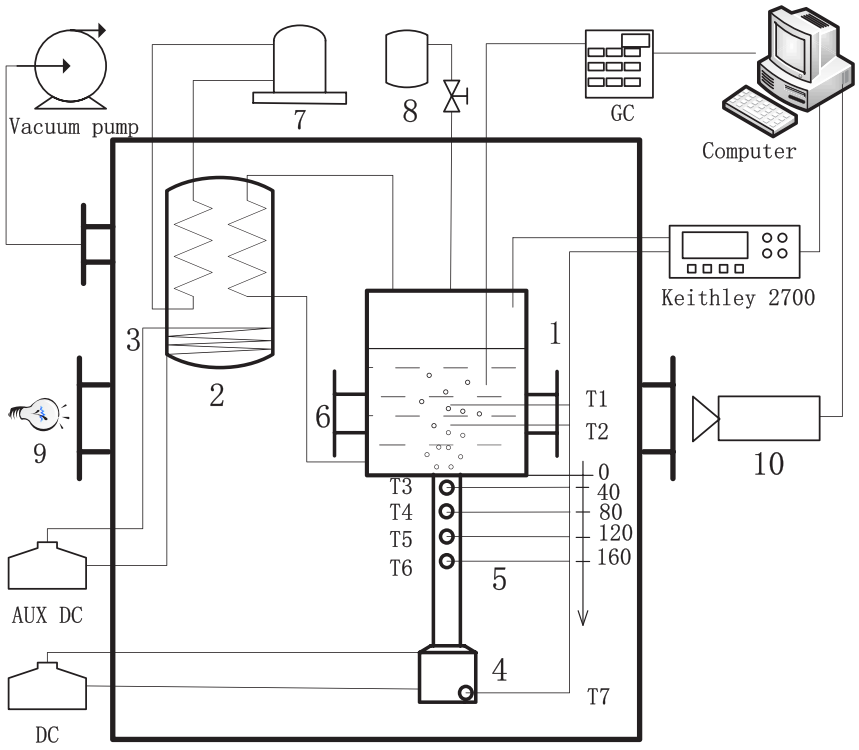

Fig. 1 – Schematic diagram of experimental apparatus: 1 – visualization boiling vessel; 2 – condenser; 3 – auxiliary electric heater; 4 – main electric heater; 5 – copper cylinder; 6 – visual windows; 7 – crycooler; 8 – refrigerant tank; 9 – illuminant; 10 – high speed camera.

During the past several decades, results from some experiments on pool boiling curves have been published and have shown the boiling phenomena in different boiling regimes. Auracher and Marquardt (2002) precisely and systematically measured entire boiling curves under both steady state and transient regimes for substances such as FC-72 under a pressure of 0.13 MPa, isopropanol under a pressure of 0.12 MPa, and water under a pressure of 0.1 MPa. Auracher et al. came to the conclusion that heating and cooling modes yielded different curves under transient conditions. In another paper, Auracher and Marquardt (2004) obtained two-phase dynamics and temperature signals on a heating surface using micro-optical probes and micro-thermocouples, respectively. From this work, the boiling mechanism in different boiling regimes was explained. Liu and Wang (2001) measured transition boiling and film boiling curves for water jets impinging on a horizontal high temperature flat plate. The heat transfer coefficient (HTC) for film boiling was obtained using a simplified two-phase flow boundary layer equation to calculate the thickness of the vapor layer. Buchholz et al. (2004) adopted a temperature-controlled heater to investigate the entire boiling curves for saturated isopropanol under a pressure of 0.104 MPa. They also studied local temperature fluctuations using micro-thermodynamics and spatial wetting dynamics with optical probes in different boiling regimes. Shirai et al. (2010) investigated the pool boiling curves on an upward flat plate in a liquid hydrogen vessel. The pool boiling curves included the natural convection regime and the nucleate boiling regime up to the CHF (critical heat flux) under pressures ranging from atmospheric to 1.1 MPa.

The CHF is an important point in a pool boiling curve. Bang et al. (2005) observed a liquid layer structure under a massive vapor clot and liquid layer-related CHF phenomenon in visualization experiments. They found that the CHF can be triggered by liquid film evaporation. Shirai et al. (2010) concluded that the occurrence of the CHF was not determined by heat flux but by the temperature in a higher pressure range. In addition, nucleate boiling directly jumped to film boiling at lower heat fluxes in the higher pressure range as the heating surface temperature reached the critical temperature prior to the occurrence of hydrodynamic instability. Meanwhile, several researchers have investigated the possible CHF mechanisms using visualization techniques. Guan et al. (2011) conducted an experiment on the saturated horizontal pool boiling of pentane, hexane, and FC-72 under pressures of 150, 300, and 450 kPa. They reported on the nucleate pool boiling curves up to the CHF and showed a clear series of images depicting the CHF boiling behavior. Ahn and Kim (2012) verified the existence of a macrolayer under a large vapor mushroom at the CHF point with a high-speed camera and proposed a new CHF mechanism for use in small heaters.

As mentioned above, many studies concerning pool boiling curves and the CHF have been conducted. However, few studies have reported on pool boiling heat transfer of R14 in the existing literature. R14 is widely used in electronics, semiconductors, laser devices and MJTR (low-temperature

mixed-refrigerant Joule-Thomson refrigerator), at temperatures ranging from 80 to 300 K (Gong et al., 2009). In our previous work, Ding et al. (2010) and Wu et al. (2011) investigated nucleate boiling heat transfer in R14 at a lower heat flux range and its mixtures with natural gas on a horizontal heating surface. As the pool boiling curves and the CHF of R14 are both of great significance academically and practically, this work focuses on experimental research into the entire pool boiling curve for R14 under a pressure of 0.1 MPa using a visualization pool boiling heat transfer apparatus. In this experiment, the pool boiling data were measured on a smooth horizontal surface and the experiment uncertainties were analyzed. The CHF point, Leidenfrost point and boiling curves in the different boiling regime are presented and discussed according to the experimental data and thermophysical properties. Moreover, the CHF data were compared with existing correlations.

2. Pool boiling experimental apparatus

Fig. 1 shows a schematic diagram of the experimental apparatus. The experimental apparatus possesses a wider operating temperature and higher heat flux limitations than that used in the present experiments, as seen in our previous work (Gong et al., 2013). This apparatus consists of a visualization boiling vessel with a horizontal copper heater surface and visual windows, a condensation system, heating units, a refrigerant tank, an image acquisition system and a data acquisition system.

The boiling vessel is a vertical stainless steel cylinder (with an inner diameter of 75 mm and a height of 100 mm). Two 12 mm thick quartz glasses were used as the visual windows to permit a maximum allowable pressure of 2 MPa. Boiling takes place on the horizontal flat surface. The heating surface is the top surface of an oxygen-free copper cylinder with a diameter of 20 mm. The copper cylinder is fixed to the bottom of the boiling vessel and sealed with Teflon. The boiling surface was lathed, and the roughness was measured with a Scan Probe Microscope (NanoscopeIIIa, USA). The 3-D structure of the boiling surface was depicted in Fig. 2. The roughness was the average of the ten measured square areas with the length of 20 μm. The measured roughness was 57.3 nm (root mean square average of the height deviations) and 46.7 nm (the arithmetic average of the absolute values of the surface height deviations). A cold light source is placed on one side of the boiling vessel to provide light to the heating surface. The high-speed camera is in front of visual window on the other side of the boiling vessel to capture videos of the boiling behavior. The camera shutter speed is 1/1000 s.

Four direct-current (DC) electric cartridge heaters were plugged into the bottom of the copper cylinder to be used as the main heater. This system can provide a maximum heat flux of 630 kW m^{-2} to the boiling surface. Various powers can be supplied by adjusting the DC voltage regulator. Four orifices were drilled in the copper cylinder at 40 mm intervals from the boiling surface. Four platinum resistance thermometers (PT100) were fixed in the orifices to provide certain temperature distributions to the copper cylinder. One PT100 thermometer was located in the bottom of the copper cylinder to determine the heating unit temperature. Another two PT100 thermometers were fixed separately to the boiling vessel to record the liquid temperature. The actual structure of the boiling vessel is shown in Fig. 3.

A mixed-refrigerant cryocooler was used to condensate the boiling vapor. A nichrome loop heater was used as an auxiliary electric heater and was intertwined on the outside surface of condenser. The pressure in the boiling vessel was held constant and saturated by the cryocooler, main electric heater and auxiliary electric heater. The boiling vessel and heating unit were well insulated inside of a vacuum chamber.

The internal pressure of the boiling vessel was measured by a pressure transducer (Druck, PMP4010), which was calibrated from 0 to 2 MPa with an uncertainty of ±0.04%. The heat transfer within the copper cylinder was assumed to be one-dimensional conduction due to the good vacuum insulation. The determination of the surface temperature and heat flux along the copper cylinder and the calculation of the uncertainties were similar to our previous work (Gong et al., 2009). Table 1 summarizes the individual standard uncertainties for each parameter.

3. Results and discussion

In this paper, extensive measurements were carried out for R14 pool boiling under a pressure of 0.1 MPa. The experimental measurements were repeated at least three times

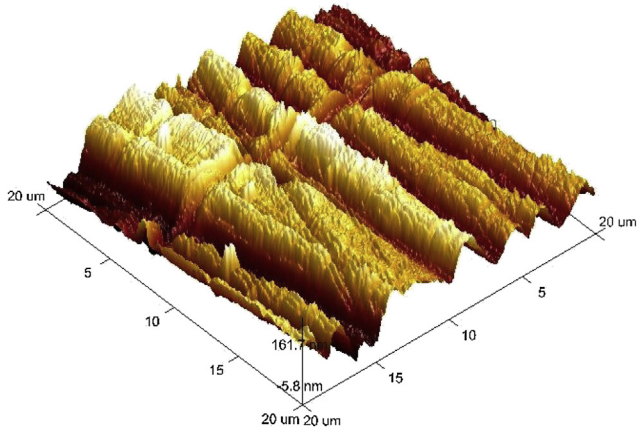

Fig. 2 – 3-D structure of the boiling surface.

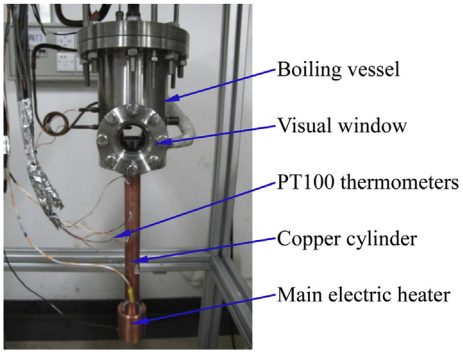

Fig. 3 – Actual structure of the boiling vessel.

Table 1 – Measurement and calculation of the uncertainties.

Parameters	Instruments	Range	Uncertainties
Temperature	PT100 thermometers	145–540 K	±0.1 K
Pressure	Pressure transducer	0–1 MPa	1000 Pa
Heat flux		35–296 kW/m^2	6.1%
Wall superheat		8–272 K	7.1%
Heat transfer coefficient		1–16 kW/m^2 K	17.4%

under the same conditions to ensure repeatability and reliability. In the experiments, the heat flux was gradually increased at intervals of approximately 37 kW m^{-2}. The system was designed to reach steady state before the heat transfer data were collected. When the pressure fluctuation is ±0.001 MPa and the temperature fluctuation is ±0.08 K for at least 10 min, the test section at this point is considered to be the steady state. The data were recorded consecutively. The measured initial point was determined from the intersection of the two curves during the experiment by increasing and decreasing the heat flux. The main heater was turned off when the temperature in the copper cylinder appeared to change, which was signified by the boiling type changing from nucleate to transition boiling. The power to the main heater was increased to obtain film boiling when the Leidenfrost point was achieved. The measured entire pool boiling curves include three regimes and two points and are presented and discussed in the following sections.

3.1. *Nucleate boiling regime*

Fig. 4 illustrates the entire pool boiling curves for R14 under a pressure of 0.1 MPa. In the nucleate boiling regime, the heat flux changed as the surface superheat temperature parameters changed, and the HTC gradually increased as the heat flux changed. From the relationship between the HTC and the heat flux in the double logarithmic coordinates, we can see that HTC changed linearly with the heat flux within the lower heat flux nucleate boiling regime, as shown in Fig. 5.

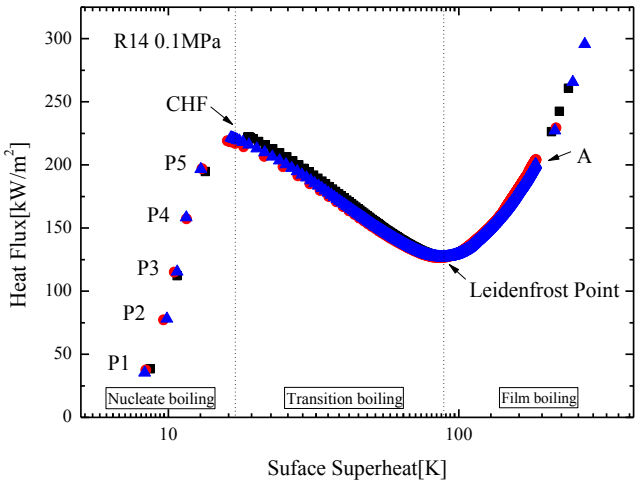

Fig. 4 – Boiling curves of R14.

Fig. 6 demonstrates the bubble behavior at different heat fluxes in the nucleate boiling regime on the heating surface. The images are selected to show the bubbles growing but not departing from the heating surface. At point 1, the single nucleation sites on the heating surface are easy to identify. The bubbles are mainly small, singular or discrete and form over the isolated nucleation sites. From the image of point 2, the bubbles form into vapor columns for the bubble departure frequency increased as the heat flux increased at a constant pressure. At certain nucleation sites, the bubbles are generated in rapid succession so that two or several bubbles at one nucleation site are connected into a vapor column.

At the high heat flux range in the nucleate boiling regime, the bubbles mutually coalesce at the time of generation and form into large bubbles. The large bubbles grow by absorbing vapor from vapor stems and finally depart from the heating surface. Meanwhile, the bubbles generated beneath these successively accompany the large bubbles grow and upward. The increase in the bubble departure diameter and the coalescence of bubbles drastically intensify as the heat flux is further increased. In addition, the bubbles that depart from the heating surface are amorphous. The progress of bubble generation, growth and departure is periodic. The rapid emission of bubbles results in good agitation for the fluid in the boiling vessel. This is part of the reason why nucleate boiling is such an efficient method for heat transfer.

3.2. *CHF*

3.2.1. *Measured data*

The transition point from the nucleate to transition boiling regime is marked by a significant decrease in the heat flux and a rapid increase in the surface superheat temperature. This point is called the critical heat flux point (CHF). The CHF means that the upper limit of the heat flux has occurred for nucleate boiling, signifying the termination of efficient heat transfer on the surface. When the CHF point arrived, the heat transfer between the bulk liquid and the heating surface was

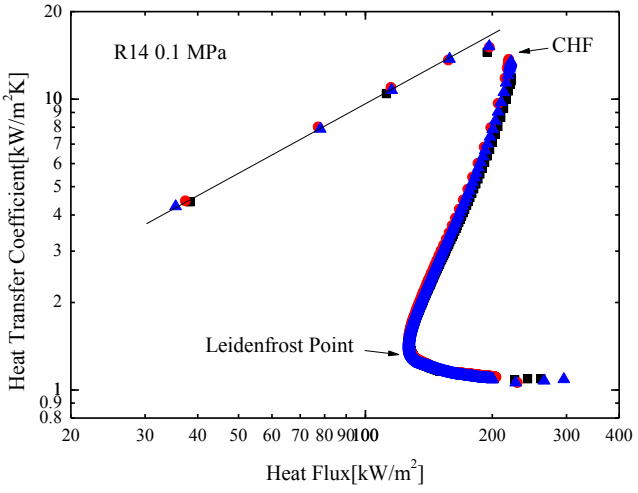

Fig. 5 – The HTC changing with the heat flux in double logarithmic coordinates.

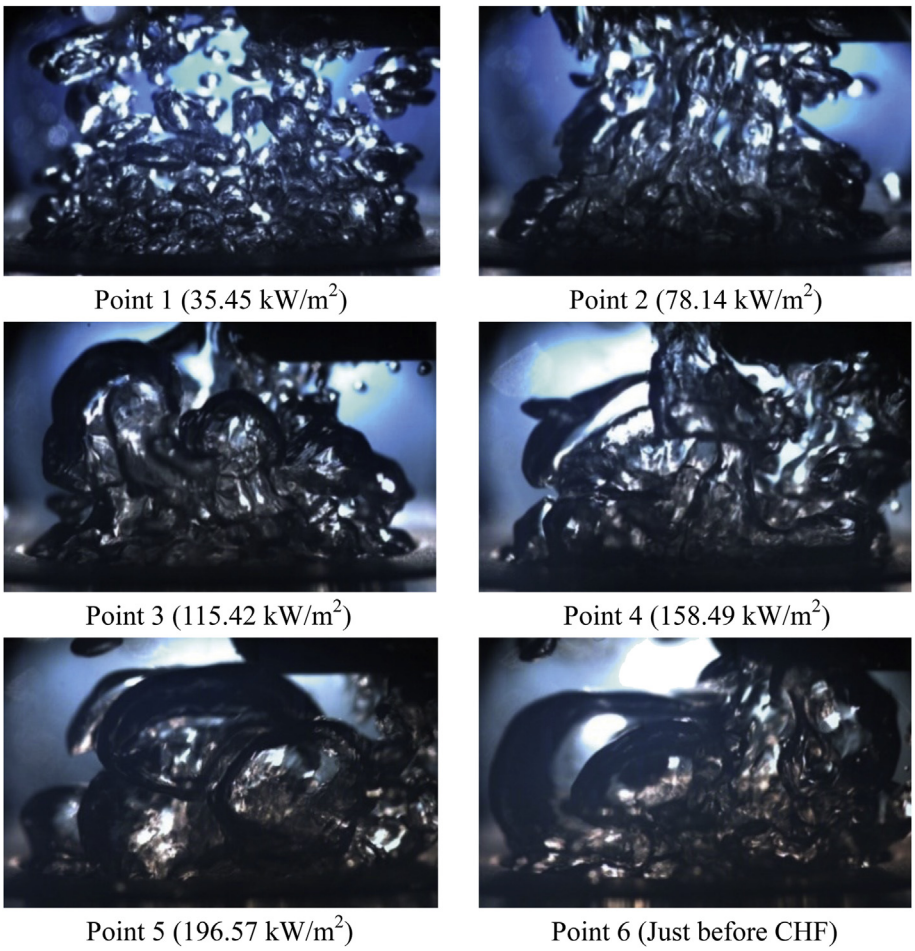

Fig. 6 – Bubble behavior at different heat fluxes in the nucleate boiling regime.

deteriorated rapidly. Meanwhile, in this experiment, a sudden temperature excursion in the copper cylinder and the heat flux decreased because of the relatively large heat capacity of the copper cylinder. The boiling automatically changed from the nucleate boiling to transition boiling without controlling the surface temperature. In this case, the boiling process was fully developed and the heat flux at the CHF point is 220.39 kW m^{-2}, which corresponded to a surface superheat temperature of 16.1 K.

3.2.2. *Comparisons with existing correlations*

The CHF is a transient semi-stable state. Therefore, most researchers analyze the CHF from two orientations, namely nucleate boiling to the CHF and transition boiling to the CHF. A variety of correlations and models have been proposed for the CHF. The existing research orientations for the CHF mechanism can be classified as: (1) a vapor blanket formed by the combination of vapor columns, (2) a Kelvin-Helmholtz instability due to the high relative velocity between the liquid and vapor emanating from the columns, (3) a dry-out of the liquid layer (Guan et al., 2011) and (4) a fractal model based on the fractal distribution of nucleation sites (Xiao and Yu, 2007). Some existing CHF correlations that have been used to predict the CHF for a horizontal surface are listed in Table 2.

A comparison of the measured CHF with the listed horizontal surface correlations is presented in Fig. 7. The deviation is that the difference between the calculated and measured CHF divided by the measured CHF. The Bailey et al. (2006) and Lienhard and Dhir (1973) correlations show good agreement with the measured data obtained in this work. Deviations of 5.41% and −7.56% are observed, respectively. For most data, the deviation between the calculated and measured data is within ±25%. The Sakashita and Ono (2009), Sakashita and Ono (2009) and Kandlikar (2011) correlations exceed ±25%. The Sakashita & Ono correlation researched the CHF under higher pressures. The Kandlikar correlation took the contact angle into account, but the specific values of the contact angle for R14 have not been determined as of the most recent public papers. The calculated value for the contact angle in this paper used the empirical value for cryogenic liquids/copper provided by Kandlikar. Hence, the actual values for the contact angle of the working fluid are in demand for available application with Kandlikar correlation.

3.3. *Transition boiling regime*

Transition boiling is located between the CHF point and the Leidenfrost point. It is characterized by a reduction in the heat

Table 2 – Existing CHF correlations for a horizontal surface.

Name	Critical heat flux correlations	Value (kW m^{-2})
Zuber (1959)	$q_{CHF,Zuber} = \frac{\pi}{24}\rho_v h_{fg}(\sigma(\rho_l-\rho_v)g/\rho_v^2)^{0.25}(\rho_l/(\rho_l+\rho_v))^{0.5}$	179.75
Lienhard and Dhir (1973)	$q_{CHF,Lienhard} = 1.14\cdot q_{CHF,Zuber}$	204.91
Haramura and Katto (1983)	$q_{CHF,Haramura}/q_{CHF,Zuber} = 5.5A^{5/8}(1-A)^{5/16}[(\rho_l/\rho_v+1)/(11/16\rho_l/\rho_v+1)^{3/5}]^{5/16}$ where $A = A_v/A_w = 0.0584(\rho_v/\rho_l)^{0.2}$	178.60
Kandlikar (2011)	$q_{CHF,Kandlikar} = 7.5(1+\cos\beta/16)[2/\pi+\pi/4(1+\cos\beta)\cos\phi]^{0.5}q_{CHF,Zuber}$	156.61
Bailey et al. (2006)	$q_{CHF,Bailey} = 1.3\cdot q_{CHF,Zuber}$	233.67
Sakashita and Ono (2009) 1	$q_{CHF,Sakashita1} = 1.128(1+\rho_v/\rho_l)^{4/5}(1+\rho_l/\rho_v)^{1/30}q_{CHF,Zuber}$	243.08
Sakashita and Ono (2009)2	$q_{CHF,Sakashita2} = 1.42(1+\rho_v/\rho_l)^{4/5}(1+\rho_l/\rho_v)^{1/30}q_{CHF,Zuber}$	306.07
Sakashita and Ono (2009)3	$q_{CHF,Sakashita3} = 4.98(\rho_l^3(\rho_l-\rho_v)gv_l^4/\rho_v\sigma^3)^{1/22}q_{CHF,Zuber}$	361.29
Guan et al. (2011)	$q_{CHF,current} = 1.837(1+\rho_v/\rho_l)^{0.25}(\rho_v/\rho_l)^{0.1}q_{CHF,Zuber}$	193.48

flux and an increase in the surface superheat temperature, as seen in Fig. 4. On other words, the heat that can be transferred is inversely proportional to the surface superheat temperature. As a result, the boiling regime is inherently unstable. The contacts of liquid–solid and vapor–liquid occurred alternatively at a certain location on the heating surface. The mechanism is similar to nucleate boiling and film boiling during wet and dry conditions, respectively. It can therefore be concluded that the HTC decreased with the heat flux, as shown in Fig. 5. The time of transition boiling process in this experiment is approximately 320 s. The speed of the decrease in the heat flux accelerated quickly before 25 s and then reduced gradually.

In Fig. 4, the heat transfer data of transition boiling are the transient point of continuous acquisition. Meanwhile, the data from the Leidenfrost point to point A in the film boiling regime also correspond to a transient point. This implies that the system cannot be maintained at steady state. In addition, the pressure in the boiling vessel started to decline after the CHF point was reached, and it increased back to the experimental pressure during low heat flux film boiling. The reason for this is that the heat transfer between the fluid and the heating surface deteriorated rapidly after reaching the CHF point, and the heat produced from the cooper cylinder cannot effectively be transferred to the liquid in the boiling vessel. Meanwhile, the boiling vessel is connected to the cryocooler through the condenser, and the condensing power provided by the cryocooler remained unchanged. This caused the liquid pressure in the boiling vessel to decline quickly and the temperature in the copper cylinder to increase rapidly. For this reason, the auxiliary electric heater is required to maintain a constant pressure after reaching the CHF point. The pressure returns to 0.1 MPa after approximately 43 min because the CHF point for the loop heaters required a longer response time.

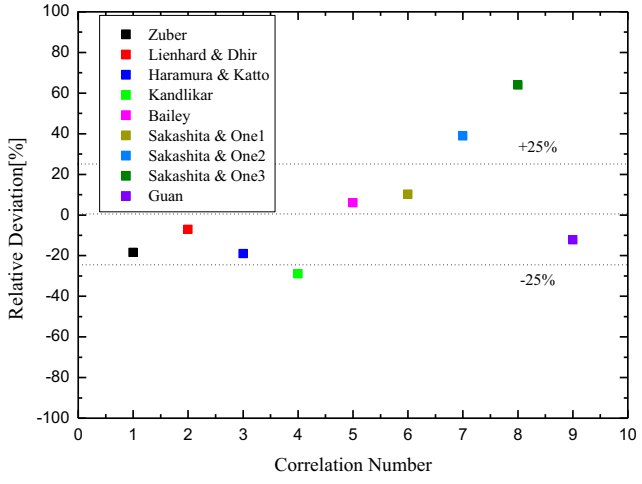

Fig. 7 – Comparison between the experimental and calculated CHF values for R14.

3.4. *Film boiling regime*

The generated bubbles buoy upward, but because they have no clear or definite escape routes, they gather around the heating surface. This caused violent boiling at the end of transition boiling regime. As the contact area of the vapor-solid increased gradually, the contact area of the liquid–solid decreased correspondingly. As the heat transfer deteriorated faster, the boiling type changed from transition to film boiling when the heating surface became completely covered in vapor. The film was a stable vapor film, and no active nucleation existed on the heating surface. The Leidenfrost point was the minimum value of heat flux in the film boiling regime and not the HTC, as shown in Fig. 5. The heat flux at the Leidenfrost point is 126.83 kW m^{-2}, which corresponds to a surface superheat temperature of 87.1 K. The calculated Leidenfrost point based on the correlation from Zuber (1959) is 105.68 kW m^{-2}, and the deviation is −16.7%, which is within the ±25% range.

In the film boiling regime, the heat flux increased with the surface superheat temperature. The HTC first decreased and then slightly increased with the heat flux. Fig. 5 shows that the growth rate of the HTC in the nucleate boiling regime is significantly greater than in the film boiling regime. The reason for this result is that the heat transfer from the fluid-solid occurred through the liquid during nucleate boiling but by conduction and radiation of a slow-flowing vapor film during film boiling. New vapor was generated continuously from the vapor–liquid interface in the film boiling regime, and the roughness and chemical composition of the heating surface have little effect on heat transfer.

4. Conclusions

In this work, an apparatus was built and modified to carry out experimental research used to visualize pool boiling heat

transfer for the entire pool boiling curves for R14 under a pressure of 0.1 MPa on a horizontal copper heating surface. The three featured boiling regimes included nucleate, transient, and film boiling, as well as the CHF and Leidenfrost points over the entire boiling curve. Some conclusions can be drawn from the present study.

(1) In the nucleate boiling regime, the surface superheat temperature and the coalesced bubble departure diameters markedly increased with the heat flux. The relation between the HTC and the heat flux in the double logarithm coordinates was approximately linear.
(2) The CHF point was achieved when temperature excursions in the copper cylinder appear at 220.39 kW m^{-2} for a surface superheat temperature of 16.1 K. The experimental data were compared with existing correlations. The Bailey and Lienhard & Dhir correlations show good agreement with the experiments with deviations of 5.41% and −7.56%, respectively.
(3) In the transition boiling regime, the heat flux decreased as the surface superheat temperature increased, and the HTC decreased with the heat flux.
(4) In the film boiling regime, the surface superheat temperature changed with the heat flux. The HTC first decreased and then slightly increased with the heat flux. The heat flux at the Leidenfrost point was 126.83 kW m^{-2}, and the corresponding surface superheat temperature was 87.1 K. The deviation was determined to be −16.7% when compared with Zuber correlation.

Acknowledgments

This work was supported by the National Natural Science Foundation of China (Grant No. 50890183)

REFERENCES

Ahn, H.S., Kim, M.H., 2012. Visualization study of critical heat flux mechanism on a small and horizontal copper heater. Int. J. Multiph. Flow. 41, 1–12.
Auracher, H., Marquardt, W., 2002. Experimental studies of boiling mechanisms in all boiling regimes under steady-state and transient conditions. Int. J. Therm. Sci. 41, 586–598.
Auracher, H., Marquardt, W., 2004. Heat transfer characteristics and mechanisms along entire boiling curves under steady-state and transient conditions. Int. J. Heat. Fluid Flow. 25, 223–242.
Bailey, W., Young, E., Beduz, C., Yang, Y., 2006. Pool Boiling Study on Candidature of Pentane Methanol and Water for Near Room Temperature Cooling. Institute of Electrical and Electronics Engineers Inc., San Diego, CA, United States.
Bang, I.Ch, Chang, S.H., Baek, W.P., 2005. Visualization of a principle mechanism of critical heat flux in pool boiling. Int. J. Heat. Mass Tran. 48, 5371–5385.
Buchholz, M., Luttich, T., Auracher, H., Marquardt, W., 2004. Experimental investigation of local processes in pool boiling along the entire boiling curve. Int. J. Heat. Fluid Flow. 25, 243–261.
Ding, L., Gong, M.Q., Bao, J.X., Sun, Zh.H., Wu, J.F., 2010. Experimental Investigation on Nucleate Pool Boiling Heat Transfer of Pure HC170, FC14 and Their Binary Mixtures. ICEC23-ICMC.
Gong, M.Q., Ma, J., Wu, J.F., 2009. Nucleate pool boiling of liquid methane and its natural gas mixtures. Int. J. Heat. Mass Tran. 52, 2733–2739.
Gong, M.Q., Wu, Y.F., Ding, L., Cheng, K.W., Wu, J.F., 2013. Visualization study on nucleate pool boiling of ethane, isobutane and their binary mixtures. Exp. Therm. Fluid Sci. 10.1016/j.expthermflusci. 2013.07.011.
Guan, C.K., Klausner, J.F., Mei, R., 2011. A new mechanistic model for pool boiling CHF on horizontal surfaces. Int. J. Heat. Mass Tran. 54, 3960–3964.
Haramura, Y., Katto, Y., 1983. New hydrodynamic model of critical heat flux applicable widely to both pool and forced convection boiling on submerged bodies in saturated liquids. Int. J. Heat. Mass Tran. 26 (3), 389–399.
Kandlikar, S.G., 2011. A theoretical model to predict pool boiling CHF incorporating effects of contact angle and orientation. J. Heat. Transf. 23 (6), 1071–1079.
Lienhard, J.H., Dhir, V.K., 1973. Hydrodynamic prediction of peak pool-boiling heat fluxes from finite bodies. J. Heat. Transf. Trans. ASME 95 (Ser C 2), 152–158.
Liu, Zh.H., Wang, J., 2001. Study on film boiling heat transfer for water jet impinging on high temperature flat plate. Int. J. Heat. Mass Tran. 44, 2475–2481.
Sakashita, H., Ono, A., 2009. Boiling behaviors and critical heat flux on a horizontal plate in saturated pool boiling of water at high pressures. Int. J. Heat. Mass Tran. 52 (3–4), 744–750.
Shirai, Y., Tatsumoto, H., Shiotsu, M., 2010. Boiling heat transfer from a horizontal flat plate in a pool boiling of liquid hydrogen. Cryogenics 50, 410–416.
Wu, Y.F., Gong, M.Q., Ding, L., Guo, P., Wu, J.F., 2011. Nucleate Pool Boiling Heat Transfer Characteristics of Tetrafluoromethane and Methane Binary Mixtures. CEC-ICMC, Spokane Washington, USA.
Xiao, B.Q., Yu, B.M., 2007. A fractal model for critical heat flux in pool boiling. Int. J. Therm. Sci. 46, 426–433.
Zuber, N., 1959. Hydrodynamic Aspects of Boiling Heat Transfer. University of California, Los Angeles and Ramo-Wooldridge Corporation, Physics and Mathematics, pp. 150–156.